Article

Volume 14, Issue 143, 2025, 128

https://doi.org/10.33263/LIANBS143.128

Facile Synthesis of Galangin-Loaded Zeolite Imidazole Framework Nanoparticles for Tumor Therapy via Induction of Cell Death in Breast Cancer Cells

Karthick Arumugam ¹, Azar Zochedh ^{1, 2}, Kaliraj Chandran ¹, Asath Bahadur Sultan ^{3,*}, Thandayarayan Kathiresan ^{1,*}

- Department of Biotechnology, Kalasalingam Academy of Research and Education, Krishnankoil, Tamil Nadu, India
- ² Center for Molecular Simulation, Biomaz Infosearch, Madurai, Tamil Nadu, India
- 3 Condensed Matter Physics Laboratory, Department of Physics, International Research Center, Kalasalingam Academy of Research and Education, Krishnankoil, Tamil Nadu, India
- * Correspondence: s.asathbahadur@gmail.com (A.B.S.); t.kathiresan@klu.ac.in (T.K.);

Received: 7.12.2023; Accepted: 7.07.2024; Published: 6.09.2025

Abstract: The primary goals of developing a novel drug delivery system are to distribute therapeutic drugs through the bloodstream in the human body and then transport them to specific therapeutic sites. In the current study, a bioactive molecule known as galangin was encased inside a metal oxide framework known as the Zeolite imidazole framework (ZIF-8) to facilitate the administration of drugs in MCF-7 cells. To initiate the synthesis of ZIF-8 nanoparticles and cargo the bioactive molecule galangin, forming GA@ZIF-8 nanoparticles. The SEM examination was used to appraise the shape of the nanoparticles, DLS and zeta potential demonstrated particle size and stability, and EDX, XRD, and FTIR analysis were used to analyze all the components and functional categories contained in ZIF-8 and GA@ZIF-8. The drug loading ability and drug release performance of ZIF-8 for the administration of galangin were investigated in phosphate-buffered saline under the influence of varied pH conditions and the targeted and controlled release of the drug. The MTT assay was used to study the dose-dependent anticancer effectiveness of GA@ZIF-8 nanoparticles on MCF-7 cells. The IC $_{50}$ values for GA@ZIF-8 nanoparticles for a time period of 24 hours were assessed to be 68.3 μ g/mL. The current research findings demonstrated that ZIF-8 allows for the regulated release of loaded galangin, and GA@ZIF-8 triggered cell death in MCF-7 cells, implying potential treatment options for breast cancer.

Keywords: galangin; MCF-7; drug delivery; ZIF-8 nanoparticles; breast cancer.

© 2025 by the authors. This article is an open-access article distributed under the terms and conditions of the Creative Commons Attribution (CC BY) license (https://creativecommons.org/licenses/by/4.0/), which permits unrestricted use, distribution, and reproduction in any medium, provided the original work is properly cited. The authors retain copyright of their work, and no permission is required from the authors or the publisher to reuse or distribute this article, as long as proper attribution is given to the original source.

1. Introduction

One of the primary issues of nanomedicine is pharmacological effectiveness. This method was greatly aided by drug delivery systems (DDSs), which encapsulate medicinal molecules, protect them from degradation, and manage the drug release mechanism [1]. Metalorganic frameworks (MOFs), an important family of nanopores crystallized organic-inorganic materials, may be created using a range of inorganic ions and organic linkers. Some of its defining features are a large surface area and porosity, simplicity of use, size and form variability, inherent biodegradability, and low toxicity [2, 3]. MOFs have lately piqued the

curiosity of the biomedical community. Researchers have made remarkable progress using MOFs in developing cutting-edge drug delivery methods. Zn-based MOFs (ZIFs) have been identified as a prominent and non-toxic subclass in biological applications [4, 5]. ZIF-8 is the most researched ZIF material because of its distinct thermochemical solidity, significant loading capability, adaptable functionality, sufficient big pore size, and drug retention and release capability [6, 7]. ZIF-8 nanocarriers may load significant quantities of cancer-fighting chemotherapeutic medicines and have a pH-sensitive targeted drug delivery characteristic [8].

Breast cancer is one of the most common malignancies in the world, with an expected 2.26 million cases in 2020, and it is the main cause of tumor death in women [9]. The global prevalence of breast cancer is likely to rise as cancer rates rise in less developed countries, although a short lifespan is not envisaged as a result. The numerous pathways are responsible for a variety of biological processes in both healthy and malignant cells, including cell proliferation, development, motility, and survival. Because of its involvement in promoting epithelial-mesenchymal transition and angiogenesis during carcinogenesis, it has been identified as a target for cancer therapies and inhibitors [10]. According to reports, flavonoids, which have been studied for their biological characteristics, such as anti-inflammatory, antiviral, antioxidant, and anti-neoplastic effects, significantly decrease a variety of cancer cells. Galangin, the active ingredient in galangal, is a natural bioflavonoid that may also be found in propolis and honey. Galangin has the chemical formula C₁₅H₁₀O₅ and a molecular weight of 270.24 g/mol. Galangin has anti-mutagenic, anti-inflammatory, anti-neoplastic, anti-cancer, anti-neurodegenerative, and anti-oxidant properties [11].

In the current study, 2-methylimidazole is coordinated with a zinc nitrate solution that provides metallic spots, resulting in ZIF-8 with a stable particle structure and therefore enhancing galangin binding. ZIF-8 particles, which also show focused therapy, transport galangin. Initial molecular docking analysis with the target protein mTOR, synthesis and physicochemical assessment of ZIF-8 and ZIF-8 loaded with galangin, ZIF-8's effective drug loading capacity, ZIF-8's potential for targeted drug release of galangin, and cytotoxicity effects on the MCF-7 cell line were all addressed in this study.

2. Materials and Methods

2.1. Molecular docking.

Molecular docking was performed through PyRx 0.8 software. At first, the 3D structure of the mTOR protein was obtained from the RCSB PDB online database. Then, the protein structure was pre-processed before performing docking. Then, ligand galangin and protein mTOR were docked in PyRx, and the interactions were investigated via the Discovery Studio tool (Biovia). The ligand and protein interaction category and interacted bond distances were analyzed in the Discovery Studio.

2.2. Reagents and chemicals.

Materials Sigma-Aldrich, India supplied the following chemicals: phosphate buffered saline (cell culture grade), 2-methylidazole (99% purity), galangin, zinc nitrate hexahydrate (reagent grade, 98% purity), methyl alcohol (anhydrous, ≥99.8%), dimethyl sulfoxide (99.7% purity), thiazolyl blue tetrazolium bromide (≥97.5% purity), acridine orange (≥98% purity), and ethidium bromide (~95%, HPLC). Fetal bovine serum (FBS), 0.25% trypsin EDTA (Gibco), and Dulbecco's modified Eagle medium (DMEM) were purchased from Invitrogen,

Carlsbad, CA, USA. All test solutions were developed using 18 MW Milli-Q water 133 (Millipore system, Burlington, MA, USA). More chemicals and analytical quality reagents were acquired from Thermo Fisher Scientific Ltd., located in Mumbai, India.

2.3. Synthesis of ZIF-8 nanoparticles.

Aqueous production at room temperature yielded zeolite imidazole framework-8 (ZIF-8) nanostructures [12]. This procedure was used because it was simple, fast, and energy-efficient. To create the zeolite imidazole framework nanoparticles, 1.48 g of zinc nitrate and 3.28 g of 2-methylimidazole were added to a 100 mL solution of methanol, and the mixture was agitated at 600 rpm at room temperature to create a white suspension. Following a two-hour incubation period, the last specimen underwent centrifugation, three rounds of methanol washing to remove any residual unreacted material, and air drying.

2.4. Load and release of galangin in ZIF-8.

In order to enhance drug loading and release, dried ZIF-8 nanoparticles were used. Once the 200 mg of dry zeolite imidazole framework (ZIF-8) nanoparticles had dissolved in 25 mL of ethanol, galangin was added. After that, the mixture was stirred for a full day at room temperature. The galangin's drug loading was assessed for a 24-hour period in 6 hrs using a BioTek ELX-800 microplate reader with an absorbance of 357 nm. The following formula was used to calculate the loading capacity of galangin on ZIF-8 nanoparticles:

percentage drug load = [(O.D at 0th hr - OD at 24th hour / O.D at 0th hour) x 100] (1) 25 mg of ZIF-8 samples containing galangin and 50 mL of PBS buffer solutions with pH values of 3.0, 5.5, and 7.4 were added to each beaker. To evenly distribute the galangin, the beakers were then shaken. GA@ZIF-8 particles were kept at a constant temperature of 37°C in order to facilitate target drug release at the specified time intervals (0 hours, 6 hours, 12 hours, 18 hours, 24 hours, 30 hours, 36 hours, 42 hours, and 48 hours). As stated before, the absorbance was ascertained after 5 mL of sample was taken on a regular basis and centrifuged at 8000 rpm. Based on the sink condition, a new addition of PBS buffer was added to the test sample.

2.5. Characterization of galangin-loaded ZIF-8 nanoparticles.

After ZIF-8 nanoparticles were created, they were examined with Fourier transform infrared spectroscopy (FTIR), X-ray diffraction (XRD), dynamic light scattering (DLS), zeta potential, and SEM-EDAX. ZIF-8 and GA@ZIF-8 were put on carbon tape for SEM (Evo18 Zeiss, Munich, Germany) and HR-TEM (JEOL Japan, JEM-2100 Plus) in order to evaluate their morphological structure. The diameter and surface charge of the nanostructures are measured by the Nanoparticle Analyzer SZ-100 (Horiba, Kyoto, Japan) using DLS and zeta potential. With K alpha kept at 0.001, the sample was scanned using the D8 Advance ECO XRD System (Bruker, Madison, WI, USA). The copper target was used for the XRD analysis, which was performed in a 3 kW X-ray tube with real-time multiple-strip solid-state detectors. Using a Shimadzu spectrometer (Nishinokyo, Japan) in transmission mode, the FTIR readings of the galangin-loaded and bare ZIF-8 nanoparticles were examined.

2.6. In vitro analysis of GA@ZIF-8 treated MCF-7 cells.

The National Centre for Cell Science (NCCS), located in Pune, Maharashtra, India, provided the breast cancer cell line MCF-7, which was acquired. Dulbecco's modified Eagle Medium (DMEM) supplemented with 5% CO₂ and 10% fetal bovine serum (FBS) was used to cultivate MCF-7 cells at 37°C. The MTT technique was used to determine the vitality of MCF-7 cells [13]. Trypsinized cells were removed from T25 confluence flasks, and 20,000 cells per well were planted in 96-well plates. Following varying doses (12.5, 25, 50, 100, and 200 μg/mL) of GA@ZIF-8, MCF-7 cells were cultured in a serum (1%) deprivation medium for a time period of 24 hrs. Tetrazolium salt was used to examine the MCF-7 cells' survival ability after exposure to nanoparticles. 10 microliters of MTT solution were applied to each well and incubated for three hours after the proper incubation time. An insoluble formazan crystal was produced as a result of the reaction between tetrazolium and the dehydrogenase reductase of living cells. After dissolving the formazan crystal in each well in 100 µL of DMSO to create purple formazan, the concentration was measured at 595 nm using a microtiter plate reader. The results were represented as a percentage (%) of control cells and were replicated three times. The double staining assay (AoEtbr) was assessed to evaluate the apoptotic death in the galangin-loaded ZIF-8 treated MCF-7 cells for the time period of 48 hr. Further, the cell migration of MCF-7 cells was assessed through the scratch test for a time period of 24 hr. The rate of apoptosis and cell migration was calculated using ImageJ software.

3. Results and Discussion

3.1. In silico molecular docking.

The protein-ligand binding interaction seems to be in an equilibrium state with complex stability, according to the Gibbs free energy (kcal/mol). The synthesis of mRNAs encoding growth factors, cell death inhibitors, angiogenesis factors, and cell growth inducers is a consequence of hyperactivated mTOR and contributes to the overall stimulation of carcinogenesis. Consequently, there is increased interest in targeting the mTOR signalling pathway as a potential drug for effective breast cancer therapy. The interaction of galangin and mTOR is shown in Figure 1.

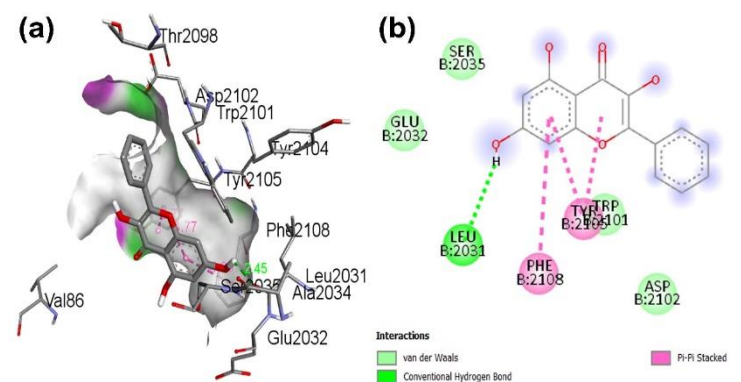


Figure 1. (a) 3d interaction with H-Bond mapping; (b) 2d interaction of galangin with mTOR.

The molecular docking results in this study indicate that galangin has a tendency to bind to the mTOR target protein with a binding energy of -8.3 (kcal/mol). It also forms one strong hydrogen bond, Leu2031, and the amino acid residues Tyr2105 (2), Phe2108, and were observed as hydrophobic Pi-orbital interactions at the active site, with bond distances of 2.44769 Å, 3.77075 Å, 4.77451 Å, and 4.831 Å, respectively. Galangin has been established

to be a more efficient therapy for breast cancer due to its beneficial interactions with proteins relevant to breast cancer.

3.2. Physicochemical characterization of nanoparticles.

A visual representation of drug loading and ZIF-8 nanoparticle production is shown in Figure 2a.

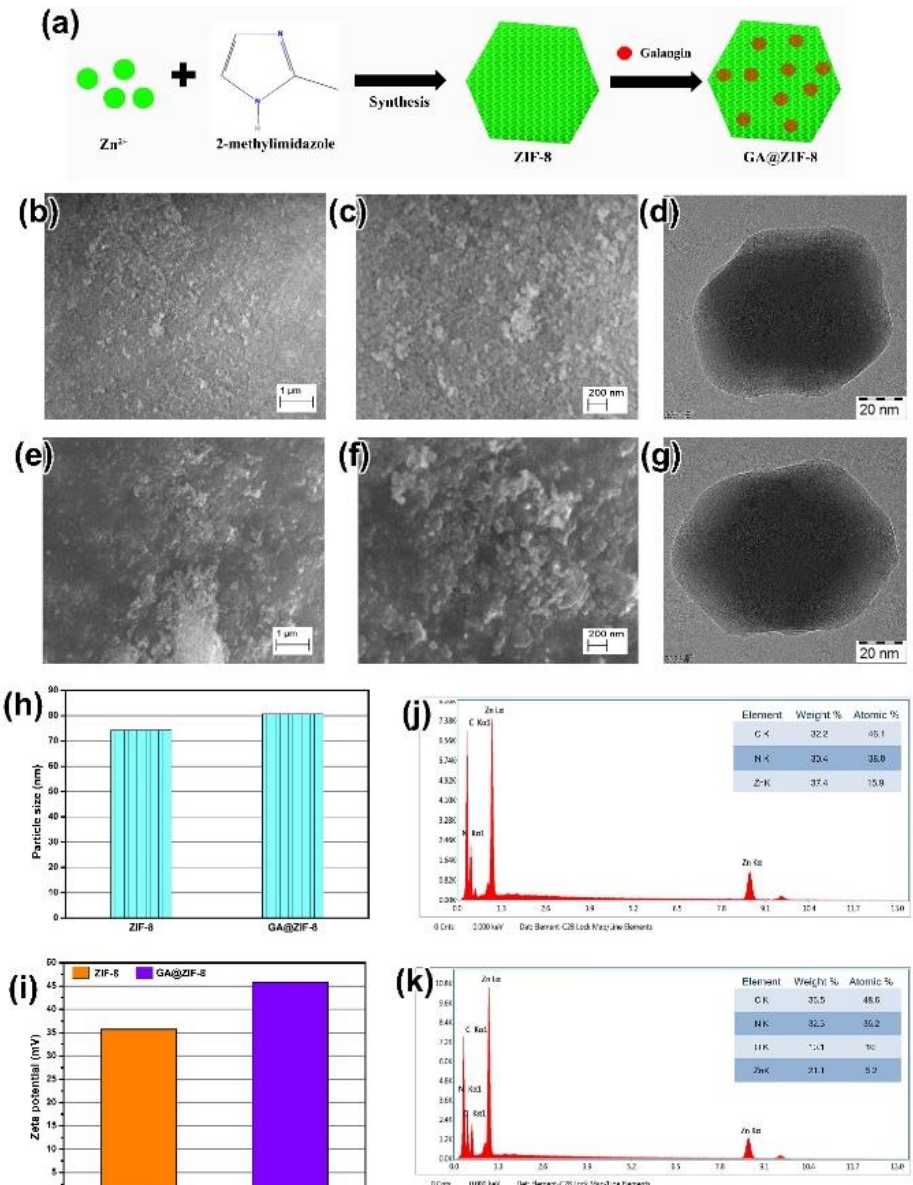


Figure 2. (a) Schematic representation of the synthesis of GA@ZIF-8; (b-d) SEM and TEM images of ZIF-8 nanoparticles; (e-g) SEM and TEM images of GA@ZIF-8 nanoparticles; (h, i) particle size and zeta potential of ZIF-8 and GA@ZIF-8 nanoparticles; (j, k) EDAX analysis of ZIF-8 and GA@ZIF-8.

The drug candidate galangin loaded onto manufactured ZIF-8 nanoparticles and the outcomes of SEM, TEM, EDX, DLS, Zeta potential studies, and elemental mapping are displayed in Figures 2 and 3. SEM and TEM analysis was used to illustrate the morphology of ZIF-8 and GA@ZIF-8. ZIF-8's morphology is shown in Figures 2 (b-d), and GAP@ZIF-8's morphology is shown in Figures 2 (e-g). It was discovered that the structure of the nanoparticles was rhombic dodecahedral. ZIF-8's diameter was measured to be 74.3 nm, whereas GA@ZIF-8's diameter was found to be 80.7 nm. The monodisperse character of nanoparticles is confirmed by the dispersity index estimates of 0.285 and 0.331, respectively [14].

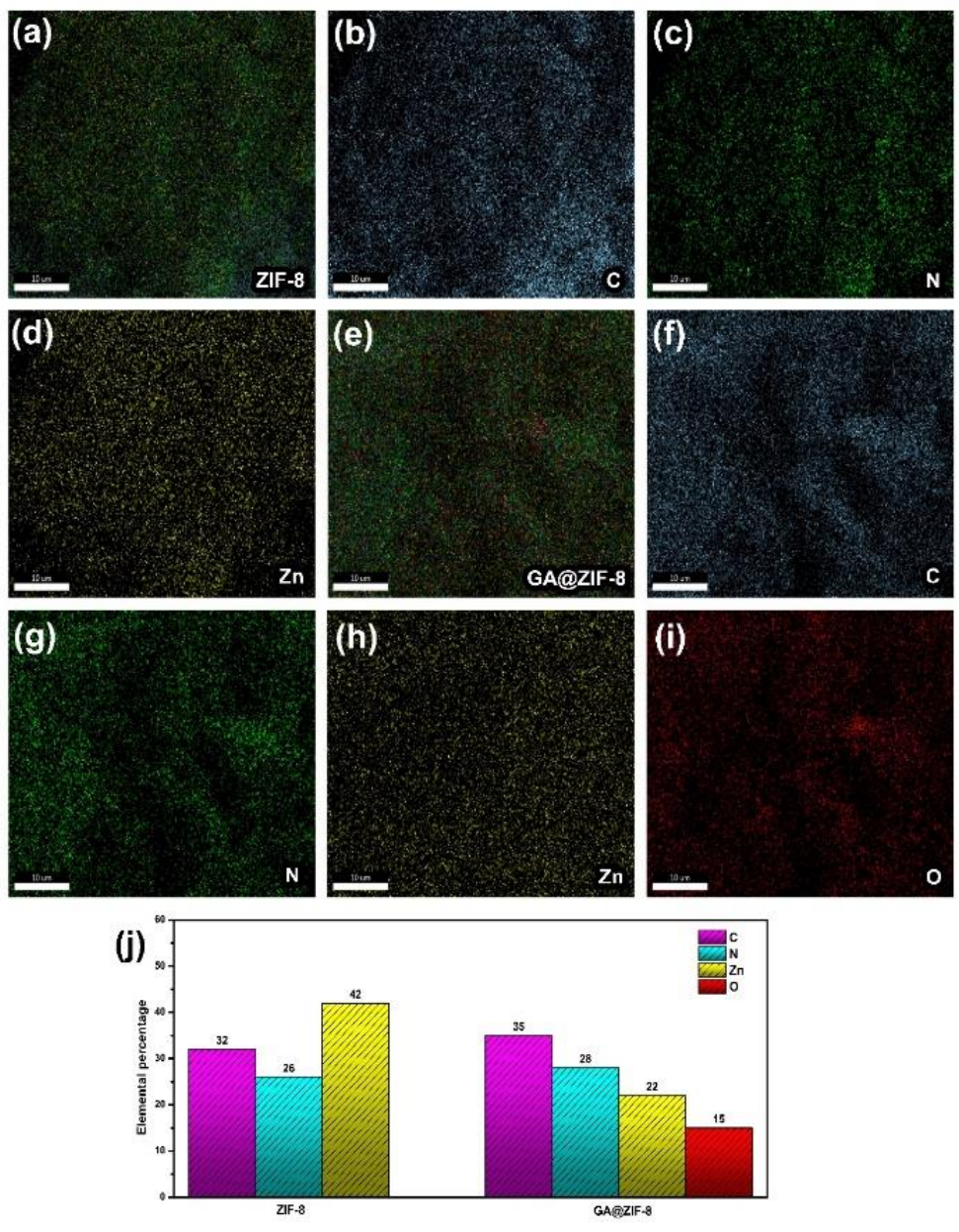


Figure 3. Elemental mapping of (**a-d**) ZIF-8 nanoparticles; (**e-i**) GA@ZIF-8 nanoparticles; (**j**) percentage of elements mapped in ZIF-8 and GA@ZIF-8.

GA@ZIF-8 is bigger than ZIF-8, which might be the result of galangin loading in ZIF-8 nanoparticles. Figure 2 (j,k) displays the results of the EDX examination. It reveals that the ZIF-8 nanoparticles have an atomic percentage of 46.1% for C, 38% for N, and 15.9% for Zn, whereas the GA@ZIF-8 has an elemental percentage of 48.6% for C, 36.2% for N, 10% for O, and 5.2% for Zn. Based on the increase in the proportion of C, N, and O and the decrease of Zn in the GA@ZIF-8 nanoparticles, it can be inferred that galangin was effectively loaded on ZIF-8 nanoparticles. Elements of ZIF-8 and GA@ZIF-8 nanoparticles are mapped to elements in Figure 3. It demonstrates that 32% of C was found in ZIF-8 nanoparticles, followed by 26% of N and 42% of Zn and that 35% of C was the most common element in GA@ZIF-8 particles, followed by 28% of N, 22% of Zn, and 15% of O. The mapping indicates that the element O in the drug-loaded ZIF-8 is attributed to the oxygen present in the structure of galangin. This indicates that ZIF-8 nanoparticles have been loaded with galangin molecules [15]. Zeta potential was used to calculate the net surface charges of ZIF-8 and GA@ZIF-8 nanoparticles; the results are displayed in Figure 2(i). ZIF-8 was shown to have surface charges of 35.7 mV

and 45.8 mV when loaded with galangin molecules. ZIF-8 nanoparticles' surface is coated with galangin, which increases the surface charge of GA@ZIF-8 relative to ZIF-8. A study on cancer has found that measuring surface charge in relation to zeta potential in cancer cells is a useful biological characteristic for determining how cells interact with certain nanomaterials [16]. Because nanoparticles are especially stable in the zeta potential range of -30 to +30 mV, they aid in the prolonged release of medications inside cells.

3.3. FTIR and XRD analysis.

The physical and chemical properties of bare ZIF-8 and GA@ZIF-8 were examined and compared. The FTIR spectrum (Figure 4a) and XRD pattern (Figure 4b) of the ZIF-8 and GA@ZIF-8 are displayed in Figure 4.

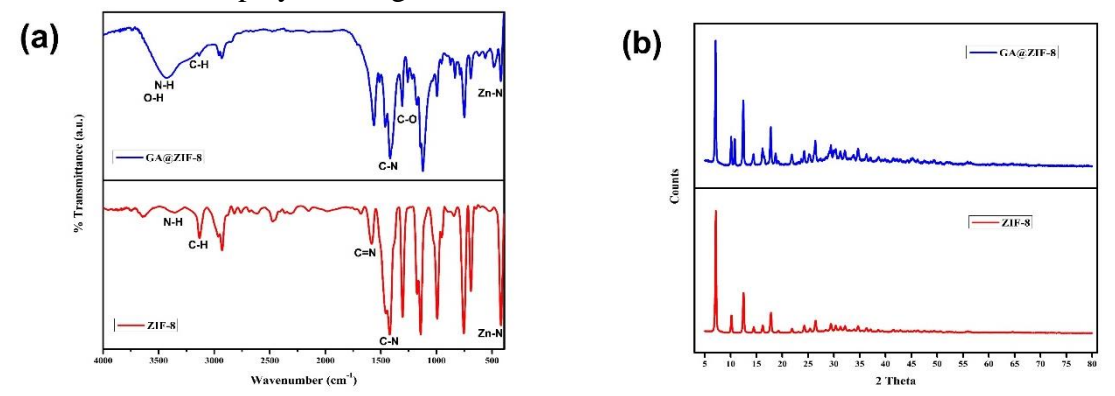


Figure 4. (a) FTIR spectrum; (b) XRD pattern of ZIF-8 and GA@ZIF-8.

The existence of functional groups in ZIF-8 and drug-loaded ZIF-8 nanoparticles was assessed using FTIR analysis. In Figure 3(a), the FTIR spectrum is shown. The peaks observed in the range of 2900 cm⁻¹ to 3200 cm⁻¹ represent the aliphatic and aromatic C-H stretching of the imidazole ring, whereas the bending (in-plane and out-of-plane) vibrations of the imidazole ring were observed at 690 cm⁻¹ to 750 cm⁻¹ and also at 940 cm⁻¹ to 1180 cm⁻¹, respectively [17–19]. N-H bending and C-H stretching are represented by the peaks that ZIF-8 nanoparticles exhibited in the range of 3371 cm⁻¹ and 3136 cm⁻¹, respectively, whereas GA@ZIF-8 presented peaks in the region of 3424 cm⁻¹ and 3135 cm⁻¹, which indicate a shift in the functional peaks [20-22]. The existence of C-N was ascertained by vibrations for ZIF-8 at 1422 cm⁻¹ and for GA@ZIF-8 at 1417 cm⁻¹, as well as the functional peak for Zn at 420 cm⁻¹ for ZIF-8 and 421 cm⁻¹ for GA@ZIF-8. The active component of the medication, galangin, exhibited vibrations of the C=C, C-H, and O-H functional groups in its FTIR spectra [23]. It is clear from Figure 4(a) that ZIF-8 nanoparticles had all of the peaks, indicating that galangin was completely loaded on them.

Figure 4(b) represents the XRD pattern of ZIF-8 and GA@ZIF-8 nanoparticles. The ZIF-8 comprehensive diffraction points, which were inducted at 2θ ranges of 7.14°, 10.19°, 12.51°, 16.13°, 17.81°, and 26.37°, were in accordance with the former study, which obligated piercing points and had been stated before. This authenticates the crystalline nature of ZIF-8 nanoparticles [24]. The XRD peaks for GA@ZIF-8, which were found at 2θ ranges of 7.06°, 10.15°, 12.41°, 16.19°, 17.77°, 26.43°, 29.52°, 32.23°, and 34.63°, illustrate the galangin peak deviations at the range of 16° and 26°. This demonstrates that galangin is crystalline in form and loaded onto ZIF-8 nanoparticles [25].

3.4. Evaluation of load and release profile of ZIF-8.

The therapeutic galangin was dissolved initially in 100% ethanol to assess the efficacy of drug loading, and then ZIF-8 nanoparticles were dispersed. Following the drug's distribution, the sample was centrifuged, the supernatant was taken out for analysis, absorbance was previously recorded at the 0th hour, OD measurements were taken at regular intervals of 6 hours, and the mixture was agitated for 24 hours. Figure 5(a) shows the drug loading percentage, and Figure 5(b) demonstrates drug release in different pH conditions.

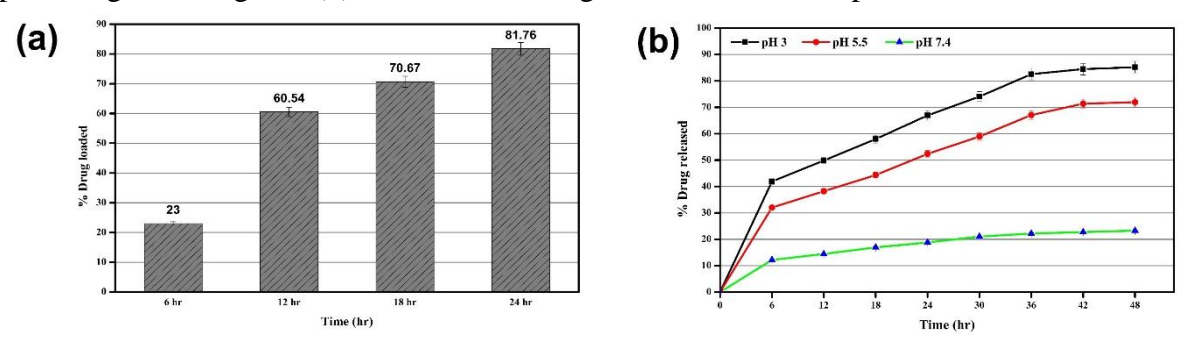


Figure 5. (a) Percentage of drug loaded in ZIF-8 at different time intervals; (b) Release percentage of galangin from ZIF-8 nanoparticles at different pH.

The proportion of drug loaded in ZIF-8 nanoparticles was then calculated using the above formula and the experimental reading, and it was determined to be 23% (6 hours), 60.54% (12 hours), 70.67% (18 hours), and 81.76% (24 hours). Depending on the time period, a rise in the proportion of drug loading was seen. After six hours, there was a marked rise in the proportion of drug load, indicating that ZIF-8 nanoparticles were capable of effectively loading drugs. It seems that the electrostatic interactions between the nanoparticles and the ZIF-8 caused the medication to be loaded [26]. To evaluate the release potential of ZIF-8 nanoparticles, three different phosphate buffer saline solutions with pH values of 3, 5.5, and 7.4 were utilized. At pH 7.4, 23.27% of the galangin molecule was released; at pH 5.5, it was 71.93%; and at pH 3, it was reported to be 85.2%. According to these results, galangin was released effectively at acidic pH levels, but only a very low percentage (23.27%) of its release occurred at neutral pH of 7.4. Although cancer cells have a pH range of 5 to 6, ZIF-8 nanoparticles show a tendency to release galangin at acidic pH, indicating the personalized release potential of ZIF-8 carriers. However, when the body's pH is 7.4, the nanoparticle ZIF-8 will produce galangin in normal cells, but it will be weak, suggesting that it won't have much of an effect on healthy normal cells. The proportion of drugs released showed that pH and time were important factors in the release of galangin.

3.5. Cell viability evaluation in MCF-7 cells.

The MTT test was performed to assess the cell viability rate when ZIF-8 and GA@ZIF-8 were injected into MCF-7 cells at different doses [27]. Figure 6 displays the treated cells' morphology and percentage of vitality. Initially, the ZIF-8 nanoparticles were subjected to treatments comprising 12.5, 25, 50, 100, and 200 μ g/mL for a whole day. Less than 2% and less than 10% of cell death were seen at ZIF-8 doses of 12.5 μ g/mL and 200 μ g/mL over a 24-hour period, respectively. This showed that ZIF-8 nanoparticles in MCF-7 cells show very minimal toxicity. The ZIF-8 nanoparticles loaded with galangin were exposed to five distinct concentrations for a duration of 24 hours. At five different concentrations, MCF-7 cells exhibited the cell viability range of 93.94% (12.5 μ g/mL), 77.25 (25 μ g/mL), 55.62 (50 μ g/mL),

 $38.22~(100~\mu g/mL)$, and $25.01~(200~\mu g/mL)$ and was represented in Figure 6b. The cytotoxic impact of GA@ZIF-8 on MCF-7 cell death was observed to be dose-dependent. The GA@ZIF-8 nanoparticle's IC₅₀ value was $68.3~\mu g/mL$ for a 24-hour treatment period. Additionally, there has been a change in the morphology of GA@ZIF-8 treated cells for 24 hr and 48 hr (Figure 6c). ZIF-8 is essential to the safe and non-toxic conventional therapy for breast cancer.

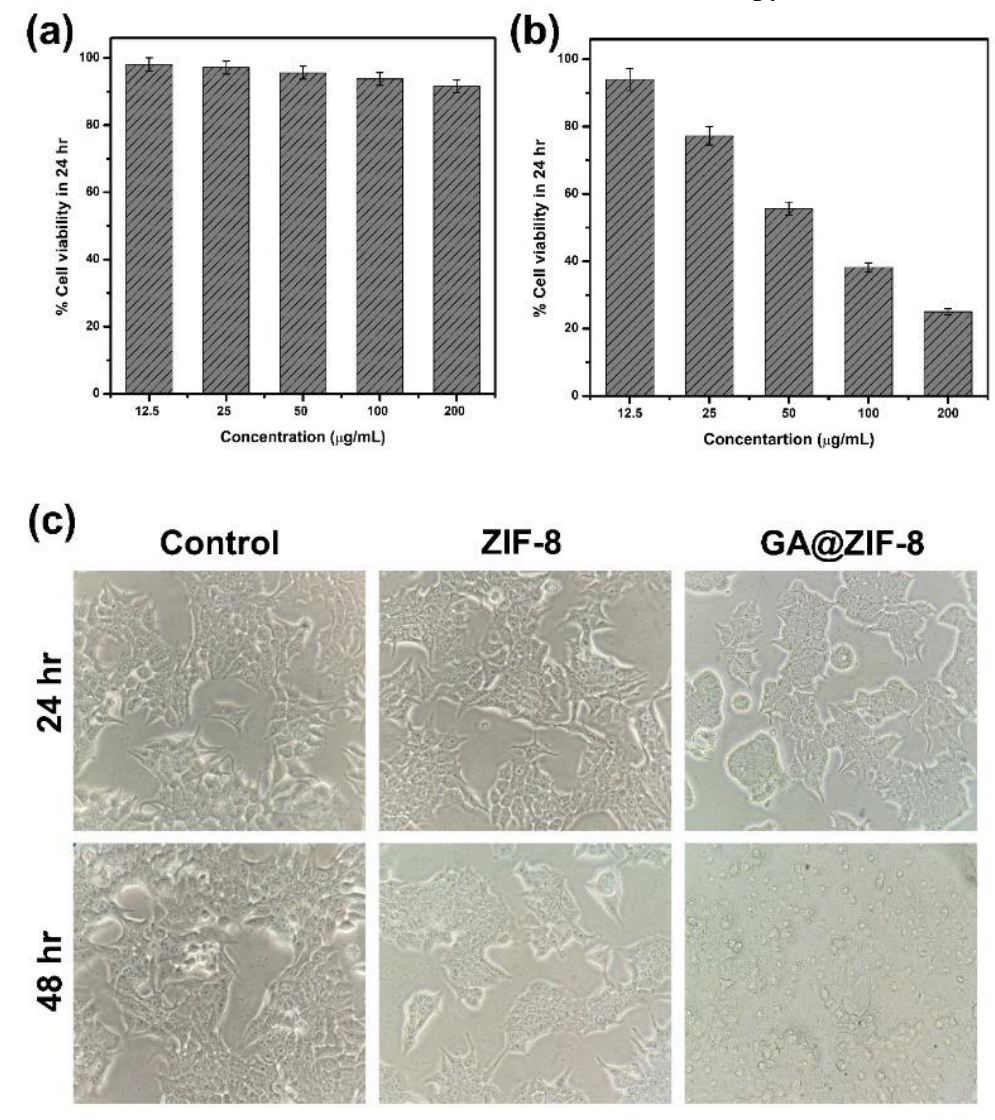


Figure 6. (a) Percentage of cell viability in ZIF-8 treated MCF-7 cells; (b) Percentage of cell viability in GA@ZIF-8 treated MCF-7 cells; (c) Morphology of untreated and treated MCF-7 cells for 24 hr and 48 hr.

3.6. Apoptosis evaluation through AoEtbr staining.

The apoptosis was assessed in GA@ZIF-8 treated MCF-7 cells for a time period of 48 hours and is represented in Figure 7. The early apoptosis, late apoptosis, and necrosis were analyzed in ZIF-8 and GA@ZIF-8 treated MCF-7 cells. After 48 hr of treatment, ZIF-8 exhibited an apoptosis rate of 6% with 2% of early apoptosis, 1% of late apoptosis, and 3% necrosis. The GA@ZIF-8 (68.3 μ g/mL) treated exhibited an apoptosis rate of 52% with 21% of early apoptosis, 12% of late apoptosis, and 19% of necrosis. Early apoptosis is a stage where the cells partially die and exhibit fluorescence in a yellowish-green color. In late apoptosis, the DNA gets fragmented and exhibits orange, whereas red indicates necrosis. The green color in Figure 7 represents live MCF-7 cells.

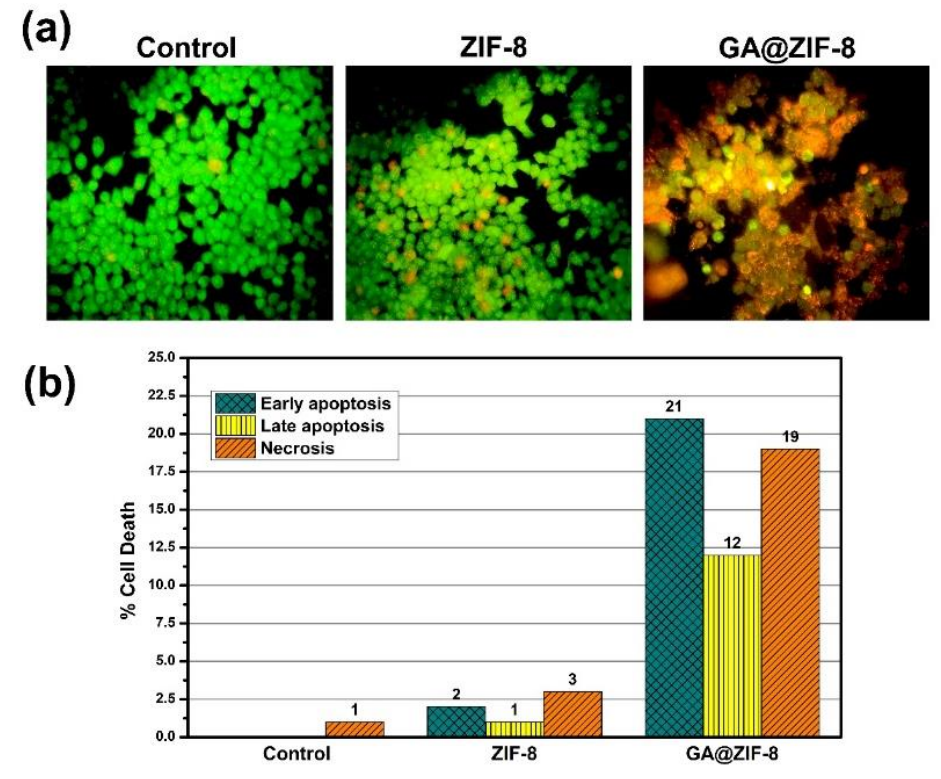


Figure 7. (a) Apoptosis with color change; (b) apoptosis percentage of untreated and treated MCF-7 cells.

3.7. Cell migration analysis.

The migration or invasion of MCF-7 cells was assessed through scratch assay, also termed a 2D cell migration assay. The migration rate of GA@ZIF-8 treated MCF-7 cells for a time period of 24 hours was represented in Figure 8. In full confluenced cells, a scratch was made using a micropipette tip, and the GA@ZIF-8 was treated for 24 hours. After 24 hours, the scratch was observed to analyze the rate of migration in galangin-loaded ZIF-8 nanoparticles treated with MCF-7 cells. The image was observed under an inverted microscope at 100x magnification. The obtained image was then processed in ImageJ software to analyze the cell migrated area of control and treated cells. From the observed area, the migration rate was calculated. The calculated cell migration rate of untreated MCF-7 cells is 52%, and GA@ZIF-8 nanoparticles treated MCF-7 cells are 14%. This shows that the GA@ZIF-8 nanoparticles inhibit the migration of breast cancer MCF-7 cells with the IC₅₀ concentration of 68.3 μg/mL.

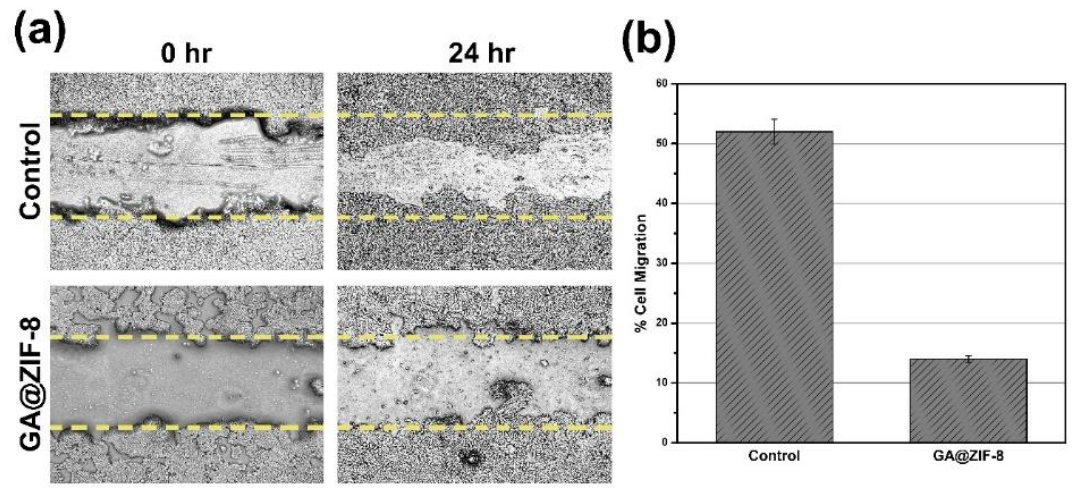


Figure 8. (a) Cell migration; (b) percentage migration in untreated and GA@ZIF-8 treated MCF-7 cells.

4. Conclusion

This study investigates the efficacy of delivering galangin-loaded zeolite imidazole framework (ZIF-8) nanoparticles to MCF-7 cells. The morphology of ZIF-8 and galanginloaded ZIF-8 nanoparticles was observed through SEM and TEM investigation. The elemental mapping and EDX analysis show the percentage of elements in the ZIF-8 particles that are bare and loaded with galangin. Strong proof that ZIF-8 was wrapped around galangin was provided by the differing proportions of C, N, Zn, and O in GA@ZIF-8 nanoparticles when compared to ZIF-8. Since the diameters of ZIF-8 and GA@ZIF-8 are smaller than 180 nm, their high bioavailability is shown by their respective sizes of 74.3 nm and 80.7 nm. The drug-loaded ZIF-8 nanocarriers were characterized using XRD and FTIR studies, verifying their crystalline structure and functional groups based on vibrational peaks. The amount of galangin released in acidic pH (cancer cells) was found to be 85.2%, but the percentage in neutral pH (normal cells) was 23.27%. This indicates that the drug release mechanism was reliant on the pH level. This suggests that the medication is more successful in delivering the medication to malignant cells and less dangerous to normal cells. The MTT test demonstrated that ZIF-8 nanoparticles had no harmful impacts on MCF-7 cells and no cytotoxic effects. The GA@ZIF-8 nanoparticles verified the dose-dependent mechanism of cytotoxicity in MCF-7 cells, with an IC₅₀ value of 68.3 µg/mL. The AoEtbr dual staining assay exhibited 52% cell death via apoptosis in GA@ZIF-8 treated MCF-7 cells, and the migration potential was inhibited in GA@ZIF-8 treated MCF-7 cells. According to our findings, ZIF-8 is a strong nanocarrier that might be used to target and release galangin for the treatment of breast cancer at various intervals and dosages with fewer adverse effects.

Author Contributions

All authors have read and agreed to the published version of the manuscript.

Institutional Review Board Statement

Not applicable.

Informed Consent Statement

Not applicable.

Funding

This work was supported by a Grant-aid from the Department of Biotechnology (DBT), BT/PR44695/NER/95/1880/2021.

Acknowledgments

The authors acknowledge Kalasalingam Academy of Research and Education for the university research fellowships. The authors also thank Biomaz Infosearch, Madurai for their technical support.

Conflicts of Interest

The authors declare no conflict of interest.

References

- 1. De Jong, W.H.; Borm, P.J.A. Drug delivery and nanoparticles: Applications and hazards. *Int. J. Nanomed.* **2008**, *3*, 133-149, http://doi.org/10.2147/ijn.s596.
- 2. James, S.L. Metal-organic frameworks. *Chem. Soc. Rev.* **2003**, *32*, 276-288, https://doi.org/10.1039/B200393G.
- 3. Azizi Vahed, T.; Naimi-Jamal, M.R.; Panahi, L. Alginate-coated ZIF-8 metal-organic framework as a green and bioactive platform for controlled drug release. *J. Drug Deliv. Sci. Technol.* **2019**, *49*, 570-576, https://doi.org/10.1016/j.jddst.2018.12.022.
- 4. An, J.; Geib, S.J.; Rosi, N.L. Cation-Triggered Drug Release from a Porous Zinc-Adeninate Metal-Organic Framework. *J. Am. Chem. Soc.* **2009**, *131*, 8376-8377, https://doi.org/10.1021/ja902972w.
- 5. Lee, J.; Farha, O.K.; Roberts, J.; Scheidt, K.A.; Nguyen, S.T.; Hupp, J.T. Metal-organic framework materials as catalysts. *Chem. Soc. Rev.* **2009**, *38*, 1450-1459, https://doi.org/10.1039/B807080F.
- Kaur, H.; Mohanta, G.C.; Gupta, V.; Kukkar, D.; Tyagi, S. Synthesis and characterization of ZIF-8 nanoparticles for controlled release of 6-mercaptopurine drug. *J. Drug Deliv. Sci. Technol.* 2017, 41, 106-112, https://doi.org/10.1016/j.jddst.2017.07.004.
- Bennett, T.D.; Cao, S.; Tan, J.C.; Keen, D.A.; Bithell, E.G.; Beldon, P.J.; Friscic, T.; Cheetham, A.K. Facile Mechanosynthesis of Amorphous Zeolitic Imidazolate Frameworks. *J. Am. Chem. Soc.* 2011, 133, 14546-14549, https://doi.org/10.1021/ja206082s.
- 8. Sun, C.-Y.; Qin, C.; Wang, X.-L.; Yang, G.-S.; Shao, K.-Z.; Lan, Y.-Q.; Su, Z.-M.; Huang, P.; Wang, C.-G.; Wang, E.-B. Zeolitic imidazolate framework-8 as efficient pH-sensitive drug delivery vehicle. *Dalton Trans*. **2012**, *41*, 6906-6909, https://doi.org/10.1039/C2DT30357D.
- 9. Wilkinson, L.; Gathani, T. Understanding breast cancer as a global health concern. *Br. J. Radiol.* **2022**, *95*, 20211033, https://doi.org/10.1259/bjr.20211033.
- 10. Dong, C.; Wu, J.; Chen, Y.; Nie, J.; Chen, C. Activation of PI3K/AKT/mTOR Pathway Causes Drug Resistance in Breast Cancer. *Front. Pharmacol.* **2021**, *12*, 628690. https://doi.org/10.3389/fphar.2021.628690.
- 11. Zhang, W.; Lan, Y.; Huang, Q.; Hua, Z. Galangin induces B16F10 melanoma cell apoptosis via mitochondrial pathway and sustained activation of p38 MAPK. *Cytotechnology* **2013**, *65*, 447-455, https://doi.org/10.1007/s10616-012-9499-1.
- 12. Siva, V.; Murugan, A.; Shameem, A.; Thangarasu, S.; Kannan, S.; Bahadur, S.A. *In situ* encapsulation of V₂O₅@ZIF-8 nanocomposites as electrode materials for high-performance supercapacitors with long term cycling stability. *J. Mater. Chem. C* **2023**, *11*, 3070-3085, https://doi.org/10.1039/D2TC03996F.
- 13. Viswanathan, T.M.; Chitradevi, K.; Zochedh, A.; Vijayabhaskar, R.; Sukumaran, S.; Kunjiappan, S.; Kumar, N.S.; Sundar, K.; Babkiewicz, E.; Maszczyk, P.; Kathiresan, T. Guanidine–Curcumin Complex-Loaded Amine-Functionalised Hollow Mesoporous Silica Nanoparticles for Breast Cancer Therapy. *Cancers* **2022**, *14*, 3490, https://doi.org/10.3390/cancers14143490.
- 14. Tran, U.P.N.; Le, K.K.A.; Phan, N.T.S. Expanding Applications of Metal—Organic Frameworks: Zeolite Imidazolate Framework ZIF-8 as an Efficient Heterogeneous Catalyst for the Knoevenagel Reaction. *ACS Catal.* **2011**, *1*, 120-127, https://doi.org/10.1021/cs1000625.
- 15. Harini, L.; Srivastava, S.; Gnanakumar, G.P.; Karthikeyan, B.; Ross, C.; Krishnakumar, V.; Kannan, V.R.; Sundar, K.; Kathiresan, T. An ingenious non-spherical mesoporous silica nanoparticle cargo with curcumin induces mitochondria-mediated apoptosis in breast cancer (MCF-7) cells. *Oncotarget* **2019**, *10*, 1193, https://doi.org/10.18632%2Foncotarget.26623.
- Mohan Viswanathan, T.; Krishnakumar, V.; Senthilkumar, D.; Chitradevi, K.; Vijayabhaskar, R.; Rajesh Kannan, V.; Senthil Kumar, N.; Sundar, K.; Kunjiappan, S.; Babkiewicz, E.; Maszczyk, P.; Kathiresan, T. Combinatorial Delivery of Gallium (III) Nitrate and Curcumin Complex-Loaded Hollow Mesoporous Silica Nanoparticles for Breast Cancer Treatment. *Nanomaterials* 2022, 12, 1472, https://doi.org/10.3390/nano12091472.
- 17. Zochedh, A.; Priya, M.; Shunmuganarayanan, A.; Thandavarayan, K.; Sultan, A.B. Investigation on structural, spectroscopic, DFT, biological activity and molecular docking simulation of essential oil Gamma-Terpinene. *J. Mol. Struct.* **2022**, *1268*, 133651, https://doi.org/10.1016/j.molstruc.2022.133651.
- 18. Priya, M.; Zochedh, A.; Palaniyandi, K.; Shunmuganarayanan, A.; Sultan, A.B. Combinatorial Effect of Syringic Acid-Pyrazinamide Adduct against Luminal Type Breast Cancer Investigated through DFT, Drug-

- Likeness, and Molecular Docking Simulation. *Polycyclic Aromat. Compd.* **2024**, *44*, 2090-2118, https://doi.org/10.1080/10406638.2023.2212105.
- 19. Chandran, K.; Zochedh, A.; Sultan, A.B.; Kathiresan, T. Observations into quantum simulation, spectroscopy, electronic properties, pharmacokinetics and molecular docking analysis of lawsone against breast cancer. *J. Mol. Struct.* **2023**, *1293*, 136280, https://doi.org/10.1016/j.molstruc.2023.136280.
- Zochedh, A.; Chandran, K.; Shunmuganarayanan, A.; Sultan, A.B. Exploring the Synergistic Effect of Tegafur-Syringic Acid Adduct Against Breast Cancer through DFT Computation, Spectroscopy, Pharmacokinetics and Molecular Docking Simulation. *Polycyclic Aromat. Compd.* 2024, 44, 2153-2187, https://doi.org/10.1080/10406638.2023.2214281.
- 21. Priya, M.; Zochedh, A.; Arumugam, K.; Sultan, A.B. Quantum Chemical Investigation, Drug-Likeness and Molecular Docking Studies on Galangin as Alpha-Synuclein Regulator for the Treatment of Parkinson's Disease. *Chem. Afr.* **2023**, *6*, 287-309, https://doi.org/10.1007/s42250-022-00508-z.
- 22. Zochedh, A.; Shunmuganarayanan, A.; Sultan, A.B. Conformational fidelity and hydrogen bond associability of L-histidine with sulfamate anion studied through XRD, quantum chemical, spectroscopic and molecular docking simulation as a cdk-4 inhibitor against retinoblastoma. *J. Mol. Struct.* **2023**, *1274*, 134402, https://doi.org/10.1016/j.molstruc.2022.134402.
- 23. Zochedh, A.; Chandran, K.; Priya, M.; Sultan, A.B.; Kathiresan, T. Molecular simulation of naringin combined with experimental elucidation Pharmaceutical activity and Molecular docking against Breast cancer. *J. Mol. Struct.* **2023**, *1285*, 135403, https://doi.org/10.1016/j.molstruc.2023.135403.
- 24. Abdelhamid, H.N.; Dowaidar, M.; Hällbrink, M.; Langel, Ü. Gene delivery using cell penetrating peptideszeolitic imidazolate frameworks. *Microporous Mesoporous Mater.* **2020**, *300*, 110173, https://doi.org/10.1016/j.micromeso.2020.110173.
- 25. Liédana, N.; Galve, A.; Rubio, C.; Téllez, C.; Coronas, J. CAF@ZIF-8: One-Step Encapsulation of Caffeine in MOF. *ACS Appl. Mater. Interfaces* **2012**, *4*, 5016-5021, https://doi.org/10.1021/am301365h.
- 26. Zilla, M.K.; Nayak, D.; Vishwakarma, R.A.; Sharma, P.R.; Goswami, A.; Ali, A. A convergent synthesis of alkyne–azide cycloaddition derivatives of 4-α,β-2-propyne podophyllotoxin depicting potent cytotoxic activity. *Eur. J. Med. Chem.* **2014**, *77*, 47-55, https://doi.org/10.1016/j.ejmech.2014.02.030.
- 27. Senthilraja, P.; Kathiresan, K. *In vitro* cytotoxicity MTT assay in Vero, HepG2 and MCF-7 cell lines study of Marine Yeast. *J. Appl. Pharm. Sci.* **2015**, *5*, 080-084, http://dx.doi.org/10.7324/JAPS.2015.50313.

Publisher's Note & Disclaimer

The statements, opinions, and data presented in this publication are solely those of the individual author(s) and contributor(s) and do not necessarily reflect the views of the publisher and/or the editor(s). The publisher and/or the editor(s) disclaim any responsibility for the accuracy, completeness, or reliability of the content. Neither the publisher nor the editor(s) assume any legal liability for any errors, omissions, or consequences arising from the use of the information presented in this publication. Furthermore, the publisher and/or the editor(s) disclaim any liability for any injury, damage, or loss to persons or property that may result from the use of any ideas, methods, instructions, or products mentioned in the content. Readers are encouraged to independently verify any information before relying on it, and the publisher assumes no responsibility for any consequences arising from the use of materials contained in this publication.